Atmospheric Research 335 (2026) 108834

Contents lists available at ScienceDirect

Atmospheric Research

journal homepage: www.elsevier.com/locate/atmosres

Investigating the predictability limit and forecast error dynamics of summer air temperatures over East Asia using the ensemble forecast dataset from ECMWF

Xuan Li [a,*], Xinyue Zhang [a], Ruiqiang Ding [b], Jianping Li [c,d], Xiaowei Huai [e,f,g]

[a] Ocean Institute of Northwestern Polytechnical University, Taicang 215400, China
[b] State Key Laboratory of Earth Surface Processes and Resource Ecology, Beijing Normal University, Beijing 100875, China
[c] Frontiers Science Center for Deep Ocean Multi-Spheres and Earth System (DOMES)/Key Laboratory of Physical Oceanography/Academy of Future Ocean/College of Oceanic and Atmospheric Sciences/Center for Ocean Carbon Neutrality, Ocean University of China, Qingdao 266100, China
[d] Laboratory for Ocean Dynamics and Climate, Qingdao Marine Science and Technology Center, Qingdao 266237, China
[e] Hunan Disaster Prevention Technology Co., Ltd., China
[f] State Key Laboratory of Disaster Prevention and Reduction for Power Grid, Changsha 410129, China
[g] Institute of Arid Meteorology, China Meteorological Administration, Lanzhou 730020, China

ARTICLE INFO

Keywords:
Surface air temperature
East Asia
Predictability
Nonlinear local Lyapunov exponent
Error growth dynamics

ABSTRACT

Accurate weather forecasts are important to society and to the economy. However, the extent to which surface air temperature (SAT) can be reliably predicted remains largely unknown. The nonlinear local Lyapunov exponent (NLLE) method takes account of nonlinearity, which governs the evolution of initial error growths in chaotic systems such as the atmosphere and ocean. Using the NLLE method and the ensemble forecasts of summer SAT derived from European Centre for Medium-Range Weather Forecasts 2009 to 2018, the upper limit of atmospheric predictability can be quantitatively estimated. This study directly applies the NLLE method to explore the upper limit of summer SAT predictability at a synoptic timescale over East Asia (EA). We investigate the upper limit and error growth dynamics for summer SAT over all EA and separately over northern EA (NEA) and southern EA (SEA). Our results show that the upper predictability limits for summer SAT over EA, NEA, and SEA are all 12 days, but there are different error growth dynamics in NEA and SEA. Considering a 15-day forecast period, we found that forecast error growths and rates are larger for SEA than for NEA during the early period, whereas the reverse is true during the later forecast period. Forecast error growths and rates over NEA and SEA also have different spatial structures. Smaller forecast error growths and lower rates occur mainly in western and northern regions of NEA throughout the forecast time, whereas southern regions of SEA have smaller forecast error growths and lower rates than northern regions. Our results will have practical guiding significance for the operational forecasts over EA.

1. Introduction

East Asia (EA) is a heavily populated region with diverse cultural and ecological systems. Accurate forecasts of surface air temperature (SAT) are beneficial to the life safety and benefit economic development (Liu et al., 2024). Multiple factors influence atmospheric circulation over EA, including tropical oceans, sea ice, and complex topography (Dickinson, 1995; Jin, 1996; Budikova, 2009), and this makes accurate SAT forecasting over EA challenging. The atmosphere is a chaotic system with high dimensionality (Lorenz, 1963, 1965; Chou, 1989), and small, local errors in the initial state from which a forecast is calculated can grow rapidly with time to eventually affect the representation of the entire atmosphere, making predictions more difficult (Thompson, 1957; Dalcher and Kalnay, 1987; Farrell, 1990). Thus, the chaotic nature of the atmosphere also limits the accuracy of weather forecasts. In recent years, weather forecasts have improved with the development of increased computing power (Xiang et al., 2020), and several multi-model forecast projects have been developed to further improve forecast accuracy. The Observing System Research and Predictability Experiment (THORPEX) Interactive Grand Global Ensemble (TIGGE),

* Corresponding author.
E-mail address: lixuan@nwpu.edu.cn (X. Li).

https://doi.org/10.1016/j.atmosres.2026.108834
Received 31 July 2024; Received in revised form 29 January 2026; Accepted 2 February 2026
Available online 3 February 2026

the Sub-seasonal to Seasonal (S2S) and the North American Multi-model Ensemble (NMME) projects have played essential roles in operational forecasting and scientific research. However, a notable deficiency of numerical models limits the credibility of forecast products and scientific studies. It is mainly because the outcomes of numerical predictions are susceptible to model uncertainties, such as incomplete understanding of atmospheric dynamics, parameterizations of sub-grid scale microphysical processes and low model resolution (Bougeault and Coauthors, 2010; Kirtman and Coauthors, 2014; Swinbank and Coauthors, 2016; Vitart and Coauthors, 2017; Liu et al., 2022). Though the model uncertainties are present and can't be removed completely, numerical outcomes are still beneficial to exploring the intricate scientific problems in atmosphere–ocean science. Many researchers have employed these numerical models to study SAT predictability at various spatial and temporal scales.

For the seasonal time scale, Stefanova et al. (2012) studied the predictability of SAT over the Southeast United States using the Global Circulation Model (GCM). Their study showed that GCM prediction skills vary seasonally and spatially. The maxima potential predictability of SAT resided outside the Southeast United States in all seasons, and the prediction skill was lowest for winter SAT. Lee et al. (2013) explored the seasonal predictability of the Asian winter temperature variability with dynamical models and a physically based statistical model. Their results showed that dynamical models had better skills for the first and second modes of the winter temperature variability, while the statistical model forecasted well for the third and fourth modes of the winter temperature variability. The difference in skills for two approaches is attributed to the external forcing factors. Liang and Lin (2018) investigated the subseasonal predictability of SAT over EA and found forecasts could be effective with a prediction lead-time of up to four weeks over East China and Northeast Asia. They pointed out that the Madden–Julian Oscillation and El Nino–Southern Oscillation had an large influence on the predictability of SAT over EA. Ehsan et al. (2019) studied potential predictability and prediction skill for SAT at seasonal timescales over the Arabian Peninsula (AP) by calculating the signal-to-noise ratio. Their results showed that dynamical models strongly overestimate summer SAT along the periphery of the AP, and underestimated in the central parts of the AP. In addition, Northern and south-western AP regions show high signal variance, while noise variance is almost uniformly distributed over the whole AP domain. Fan et al. (2020) used the maximum signal-to-noise (MSN) empirical orthogonal function (EOF) method to analyze the most predictable patterns of the wintertime 2-m air temperature (T2m) in the extratropical Northern Hemisphere. Results showed that the predictable modes of the wintertime T2m exhibited different patterns over the Arctic, the Pacific–North America and the Tibetan Plateau.

For the longer time scale, Salvi et al. (2017) studied the forecast skills of decadal temperature over 7 regions in continental United States. Their results showed that dynamical models had mediocre potential skills for most regions. And different magnitudes of unconditional biases were present in distinct regions, which were responsible for the skill scores. Monerie et al. (2018) evaluated the performance of the DePreSys3 prediction system for predicting summer SAT over North EA and found that high skills for SAT were mainly over North East Asia, the North Atlantic Ocean and Eastern Europe. In addition, the substantial skill in DePreSys3 is owing to the ability of the decadal prediction system to simulate the circumglobal teleconnection pattern variability. Verfaillie et al. (2021) assessed the reliability of decadal climate predictions of near-surface air temperature over 30 different regions, including 21 land regions and 9 ocean regions. Results showed that most regions exhibited different reliability of near-surface air temperature for forecast year 1 and forecast years 1–5. Müller et al. (2012) investigated the forecast skills of multi-year seasonal means of SAT. The result showed that winter SAT had high skills over northern Europe, while the summer to autumn SAT had high skills over central and south-eastern Europe. In addition, Jia and DelSole (2012) pointed out that the land SAT was significantly predictable on multi-year time scales, ranging from 3 to 20 years, depending on models.

Although previous studies have made a number of important advances that deepen our understanding of SAT predictability, the research still leaves several limitations. Firstly, the predictability limits of SAT are still not quantitatively determined. It mainly can be attributed to the research method. The signal to noise method is prevailing in the SAT predictability. However, this method could qualitatively study the predictability, but fail to quantitatively estimate it. Secondly, some studies employed the statistical approaches to investigate the SAT predictability, which may lead to unreliable results. Since statistical approaches are constructed based on a linear perspective, without the considering the chaotic nature of atmosphere. Furthermore, some studies used the dynamical models to study the SAT predictability. However, due to the inherent mode errors and inaccuracies in the numerical model itself, the research results also exhibit a significant uncertainty.

The Lyapunov exponent (LE) describes qualitative and quantitative dynamic behaviors and is related to the average rate of divergence or convergence of nearby orbits in phase space. The LE is a classic method used in research into the predictability of dynamic systems (Wolf et al., 1985). The finite time (or local) LE has been proposed for studying local atmospheric predictability. Many studies have used the local LE to study the dynamics of error growth and local predictability (Nese, 1989; Yoden and Nomura, 1993; Vannitsem, 2017). However, similar to the SV method, the local LE is calculated from the tangent linear model and hence represents the average error growth rates only in the linear regime. To overcome this limitation, Ding and Li (2007) proposed the nonlinear local Lyapunov exponent (NLLE), based on the local LE. The NLLE differs from the local LE because it is obtained by integrating the primitive equations without linearizing the primitive equations. Therefore, the NLLE depends on the initial conditions, initial error, and integration time and can capture error dynamics in the linear and nonlinear regimes (Ding and Li, 2007). The NLLE method effectively estimates the intrinsic predictability of chaotic systems. There are explicit governing equations for chaotic systems; however, the real atmosphere has no explicit governing equation, suggesting that direct application of the NLLE method to studies of atmospheric predictability may be inappropriate. To quantify atmospheric predictability, Li and Ding (2011) calculated the NLLE by searching for local dynamic analogues in the observation data. If the initial and evolutionary distances between a state and a reference state are small within a finite time interval, then the state is considered to be the local analog of the reference state. The predictability can then be quantified. Algorithms based on this NLLE technique have been widely applied in studies of atmospheric and oceanic predictability (Ding et al., 2010, 2011; Li and Ding, 2013; Ding et al., 2016; He et al., 2021). Algorithms that search for local dynamic analogues help to facilitate the widespread application of NLLE for the real atmosphere and ocean. Comparing with the signal to noise method, statistical approaches and dynamical models, the NLLE method not only overcomes the limitation of qualitative examinations, but also takes account of the nonlinearity owing to the chaotic nature of atmosphere. In addition, the NLLE method can use observation data to quantify the predictability limits of atmosphere, which avoids the model uncertainties. By contrast, the NLLE method takes advantage over the signal noise method, statistical approaches and dynamical models in estimating predictability limit of atmosphere.

It is therefore useful to investigate direct application of the NLLE method to research into atmospheric predictability. In practice, the ensemble forecast technique provides another way to calculate the NLLE without searching for local dynamical analogues. In an ensemble forecast, the initial conditions for each ensemble member represent perturbations around the true state of the system at the initial time. The dynamic evolutions of the initial perturbed conditions remain close to the trajectory of the true conditions at the beginning of the forecast period. Therefore, at different lead-times, multiple forecasts can be

obtained by integrating the initial perturbed forecasts. This suggests that the NLLE can be calculated directly from perturbed forecasts and observation data. This allows atmospheric predictability to be quantified using the NLLE method without searching for local dynamic analogues.

This study attempts to apply the NLLE method to investigate summer SAT predictability over EA and to quantify its upper limit. Many previous studies are focused on the SAT predictability at seasonal and decadal time scales. Few studies are devoted to the SAT predictability at synoptic scales, especially its predictability limit.

Therefore, we focus here on summer SAT predictability limit at the synoptic timescale. For this reason, the ensemble forecast dataset will be used in this study. Many studies have evaluated the forecast accuracy of TIGGE products from different numerical centres, and concluded that the ensemble forecast dataset from the ECMWF has the highest level of skill, using the root-mean-square error, spatial correlation, bias score, spread and continuous ranked probability skill score (Froude, 2010; Su et al., 2014; Rohini and Rajeevan, 2023). In addition, the ensemble forecasts from the ECMWF have more ensemble members, longer forecast ranges, higher resolution comparing to other centres. Therefore, based on the above considerations, we will employ the ensemble forecast dataset from the ECMWF to quantify the predictability limit in this study. We also investigate forecast error growth dynamics for summer SAT over EA. Given that many previous studies have pointed out that variations of geographic areas would significantly impact on SAT predictability (e.g. Liang and Lin, 2018; Ehsan et al., 2019; Fan et al., 2020), we will divide the EA into two areas, the northern EA and southern EA to study the summer SAT predictability.

The remainder of this paper is organized as follows: in Section 2, we describe the ensemble forecast data and the NLLE methodology; the predictability of SAT over EA and error dynamics are assessed in Section 3; and some discussion and conclusions are presented in Section 4.

2. Data and methodology

2.1. Ensemble forecast data and verification data

The TIGGE project includes ensemble forecast data from 13 numerical centers, including from ECMWF, National Centers for Environmental Prediction (NCEP), China Meteorological Administration (CMA). It is recognized that the ECMWF center has more skillful performances than other centers (Swinbank and Coauthors, 2016; Rohini and Rajeevan, 2023). It is attributed to the data assimilation technique, ensemble forecast scheme, model resolution and so on. Therefore, ensemble forecast data from ECMWF will be used in this study. The ECMWF forecast ensemble has 50 members, comprising 1 control member and 50 perturbed members. The prediction lead-time is up to 360 h, corresponding to a synoptic timescale. Different meteorological variables, including temperature, wind, specific humidity and geopotential height, can be obtained from the ensemble forecast output. In this study, we analyzed and quantified predictability of the daily mean air temperature at the height of 2 m. The ensemble forecast data for summers (June, July, and August) from 2009 to 2018 are used in this study. It should be noted that the ensemble forecast data for summer 2013 over EA are corrupt. Therefore, a total of 9 years of ensemble forecast data are used in this study. The horizontal resolution is $0.5^\circ \times 0.5^\circ$, and the verification data are from the ERA-interim reanalysis, with a resolution of 0.5° (Dee and Coauthors, 2011). ERA-interim reanalysis was released in 2011 and discontinued in 2019. The latest version of ECMWF's reanalysis product is the fifth generation European Center for Medium Range Forecasting Reanalysis (ERA5, Hersbach et al., 2020). This ERA-interim reanalysis includes a large variety of 3-hourly surface parameters, describing weather as well as ocean-wave and land-surface conditions, and 6-hourly upper-air parameters covering the troposphere and stratosphere. In this study, we employed the air temperature analysis at the height of 2 m as the verification data. The temporal and spatial resolution of air temperature analysis is 6-hourly and 0.5°. It should be pointed out that we have compared the ERA-interim and ERA5 datasets. We found that the conclusions remain unaffected regardless of whether ERA-Interim or ERA5 data is used. Therefore, the results throughout the study are obtained based on the ERA-interim reanalysis.

2.2. NLLE methodology

Many studies have investigated predictability for theoretical chaotic models and atmospheric and oceanic systems. However, most studies have employed linear methods such as the SV or the local Lyapunov exponent to research the predictability. Linear methods are applicable only when the initial error is infinitesimal; however, the atmosphere is chaotic and the initial error is always finite. This means that there are limitations associated with using linear methods to study atmospheric predictability. The NLLE method (Ding and Li, 2007) takes account of nonlinearity and captures the error dynamics in both the linear and nonlinear regimes. It has been widely applied in research into atmospheric and oceanic predictability. The following paragraphs present a detailed description of the NLLE method.

The dynamic evolution of an n-dimensional dynamic system is governed as follows:

$$\frac{d}{dt}\boldsymbol{x}(t) = F[\boldsymbol{x}(t)] \tag{1}$$

where $\boldsymbol{x}(t) = (x_1(t), x_2(t), \ldots x_n(t))^T$ is the state vector. The growth of the initial errors $\delta(t_0)$ can then be expressed as follows:

$$\boldsymbol{\delta}(t_0+\tau) = \boldsymbol{\eta}(\boldsymbol{x}(t_0), \delta(t_0), \tau)\delta(t_0) \tag{2}$$

where $\boldsymbol{\delta}(t_0) = (\delta_1(t_0), \delta_2(t_0), \ldots \delta_n(t_0))^T$ is the initial error, and $\boldsymbol{\delta}(t_0+\tau) = (\delta_1(t_0+\tau), \delta_2(t_0+\tau), \ldots \delta_n(t_0+\tau))^T$ is the error at time $t_0+\tau$.

$\eta(x(t_0), \delta(t_0), \tau)$ is the nonlinear error propagator. Based on Eq. (2), the NLLE is defined as

$$\lambda(\mathbf{x}(t_0), \boldsymbol{\delta}(t_0), \tau) = \frac{1}{\tau}\ln\frac{\|\boldsymbol{\delta}(t_0+\tau)\|}{\|\boldsymbol{\delta}(t_0)\|} \tag{3}$$

The notation $||.||$ represents the 2- norm of a vector. Where $\lambda(\boldsymbol{x}(t_0), \boldsymbol{\delta}(t_0), \tau)$ depends on the initial state in phase space, $\boldsymbol{x}(t_0)$, the initial errors, $\boldsymbol{\delta}(t_0)$, and the integration time, τ. The NLLE represents the average nonlinear growth rate as the initial error evolves between time t_0 and time $t_0+\tau$.

The ensemble-average NLLE global attractor for the dynamic system is given by:

$$\bar{\lambda}(\boldsymbol{\delta}(t_0), \tau) = \frac{1}{N}\int_{\Omega}\lambda(\boldsymbol{x}(t_0), \boldsymbol{\delta}(t_0), \tau)dx$$

$$= \langle\lambda(\boldsymbol{x}(t_0), \boldsymbol{\delta}(t_0), \tau)\rangle_N \tag{4}$$

where $\langle\rangle_N$ is the average from an ensemble that includes sufficient samples, with size N. The mean relative growth of the initial error (RGIE) can therefore be obtained as follows:

$$\bar{E}(\boldsymbol{\delta}(t_0), \tau) = \exp(\bar{\lambda}(\boldsymbol{\delta}(t_0), \tau)\tau) \tag{5}$$

$\bar{E}(\boldsymbol{\delta}(t_0), \tau)$ grows with time and will eventually reach saturation level. While $\bar{E}(\boldsymbol{\delta}(t_0), \tau)$ is at the saturation level, the error growth is in the nonlinear regime and predictability is lost completely. Prior to the saturation level being reached, there is predictability. Therefore, the predictability limit for chaotic systems is defined as the time taken by $\bar{E}(\boldsymbol{x}(t_0), \tau)$ to reach 99% of its saturation level (Ding et al., 2011).

3. Results

3.1. Upper predictability limit of SAT over EA

Fig. 1 shows the climatology for summer SAT over EA. The study area spans 30 latitudes, and SAT is higher in the southern regions than in the northern regions. Liang and Lin (2018) explored the SAT predictability over EA, and found that East China and Northeast Asia have higher forecast skills. It is evident that SAT predictability over the EA region exhibits pronounced spatial heterogeneity. Numerous factors can modulate the mechanisms governing error growth dynamics. In our opinion, the background SAT temperature climatology is a key influence factor. From Fig. 1, to North of 40°N, summer SAT climatology is relatively lower, whereas to south of 40°N, it is higher. Therefore, using 40°N as the dividing line, we partition East Asia into northern EA (NEA) and southern EA (SEA). The hottest region lies in the southeast and south of the SEA, where the SAT reaches up to 28 °C. The coldest region lies in the northwest of the NEA, where the SAT is <20 °C. The SAT conditions are different in these two areas, so the error growth dynamics for these areas may also differ. Therefore, we assess SAT predictability and error growth dynamics separately over all EA, NEA, and SEA.

First, we will quantitatively estimate the predictability of SAT over all EA using the NLLE method. The ensemble forecast data includes nine years of forecasts from 1 June to 31 August (from 2009 to 2018, except 2013) and the prediction lead-time is up to 15 days. We calculated the NLLE from the ensemble forecast data and EAR-interim data for each year. Fig. 2a shows that the NLLEs for each year have relatively small spread, implying that the error growth dynamics were similar for the nine years. The NLLE decreases with time and remains roughly unchanged during the later period. In practice, NLLE varies over three different stages; i.e., the sharp decreasing, stable decreasing, and minor change stages. During the first stage, the initial error growth rates range from 0.3 to 0.4. However, at the end of the 2nd day, the error growth rates decrease to ~0.1. NLLEs for all nine years have a decreasing shape. During the second stage, there is a stable decrease in the error growth rates. This stage lasts for about 10 days. At the end of the second stage, the error growth rates are roughly 0.05. The total drop in amplitudes of the error growth rates is smaller over this second stage than that over the first stage. During the third stage, the error growth rates remain largely unchanged. The phenomenon of variations of NLLEs is determined by the inherent property of error growth dynamics. Generally, smaller error magnitude leads to higher rate of error growth, and vice versa. At initial time, the size of initial ensemble perturbations is quite small, thus the rate of error growth maintains high. As the forecast time increases, the errors grow large, and the rate of error growth decreases. Analysis of NLLEs for individual years shows that they have similar variations, indicating that the error growth dynamics are similar for each of these years, which means that the predictabilities for the SAT should also be similar for each of these years. We calculate the growth of the forecast error for each year from the NLLEs. Fig. 2b shows variations in the average forecast error growth with time over nine years. To quantify the predictability, we must determine when the forecast error growth reaches the saturation level. The rationale behind defining the saturation level is that the chosen time length should be within the saturation phase. In addition, considering the whole forecast time length in this study is not too long, only 15 days, thus the saturation level period should try to choose later days of the whole forecast time. In this study, the saturation level is the average of the forecast error growths for the last 5 days of the third stage. Fig. 2b shows that the forecast error growth increases with time during the first two days. From day 1 to day 2, forecast error growth increases rapidly. From day 3 to day 13, the forecast error growth increases slowly, after which the forecast error growth remains unchanged. In practice, the forecast error growth saturates on the thirteenth day, indicating that the error growth enters the random regime, and predictability is lost completely (Ding and Li, 2007; Ding et al., 2011). Therefore, the average upper limit for SAT predictability over EA is 12 days. We also found that, for each individual year, the upper limit for SAT predictability is roughly 12 days (figures not shown). Therefore, effective forecasts of summer SAT over EA extend to a lead-time of 12 days.

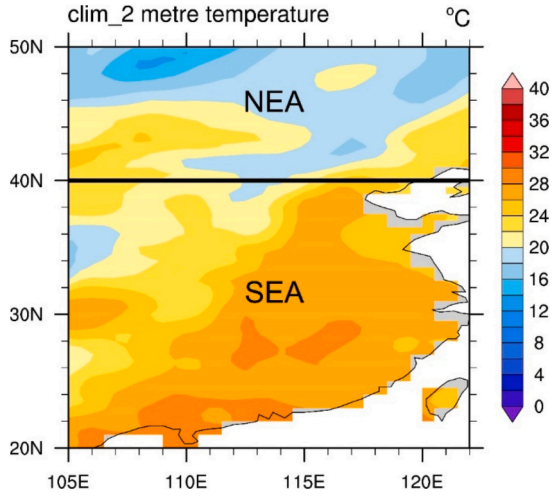

Fig. 1. Climatology of summer surface air temperature during summer (June, July August) 1981–2010 (units: °C) over East Asia. The black line is the dividing line between northern East Asia (NEA) and southern East Asia (SEA).

3.2. Forecast error growth and its rates of SAT over EA

Following our estimate of the predictability of summer SAT over all EA, we now analyze the predictabilities and error dynamics for summer SAT over the NEA and SEA. Fig. 3 shows the variations in NLLEs for NEA and SEA with lead-time. NLLEs for NEA and SEA show similar variability to that seen for all EA. That is, NLLEs for these two areas experience three different stages: the sharp decreasing stage, the stable decreasing stage, and the minor change stage, respectively. However, the error growth dynamics of these two areas differ from each other, and from those for all EA. During the first stage, the initial error growth rates for SEA are higher than those for NEA. NLLEs for SEA at the initial time range from 0.38 to 0.50, with an average value of 0.45, whereas NLLEs for NEA at the initial time range from 0.14 to 0.30, with an average of 0.21. Error growth rates are higher for SEA than for NEA throughout the first stage and remain higher at the end of the first stage. NLLEs for both areas continue to decrease during the second stage, and NLLEs remain larger for SEA than for NEA. However, around the fifth day, the average NLLE for NEA exceeds that for SEA. From this point until the third stage, the average NLLE for NEA remains higher than that for SEA. Therefore, the error growth rates are higher for NEA than for SEA during the second and third stages. The error growth rate for all EA is between those for NEA and for SEA for all forecast lead-times. At the initial time, the average initial error growth rate for all EA is 0.37, which is higher than that for NEA but lower than that for SEA. However, during the second stage, the error growth rate for NEA gradually exceeds that for SEA. Correspondingly, the error growth rate for all EA is higher than that for SEA but lower than that for NEA during the second stage. The differences between the error growth rates in EA, NEA, and SEA show that SEA contributed more than NEA to the forecast error growth for EA during the first 4 days, while NEA made a greater contribution than SEA after the first 4 days.

The above analysis focuses on the error growth rates averaged over EA, NEA, and SEA. However, investigating spatial variations in error growth rates may provide more regional information. Fig. 4 illustrates how the spatial distributions of NLLEs in NEA vary with time, and shows that the NLLEs over NEA are largest during the first day. Most regions have positive NLLEs, and those regions with negative NLLEs are located

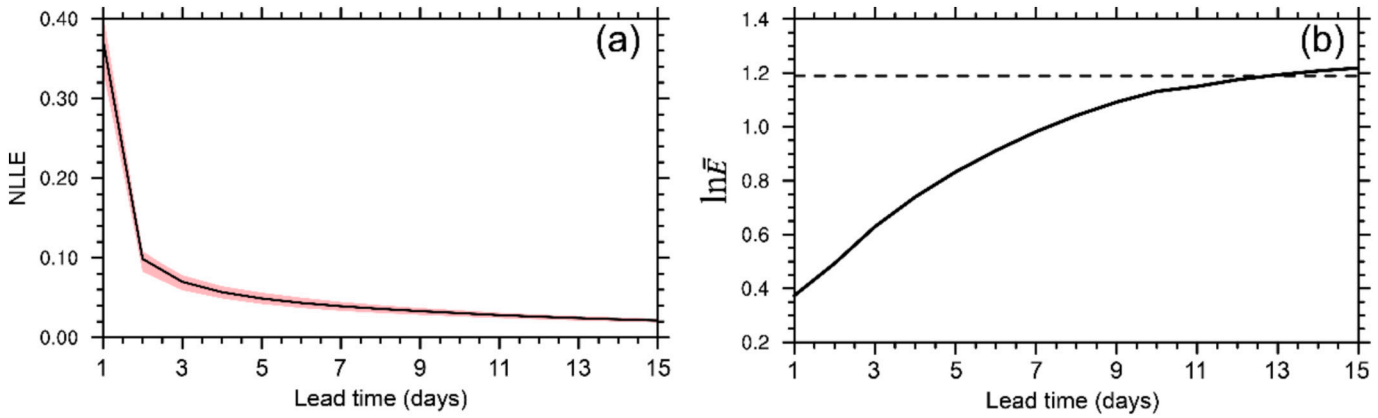

Fig. 2. Variations in the average (a) nonlinear local Lyapunov exponent (NLLE) and (b) forecast error growth (natural logarithm scale) as a function of forecast lead-time. Red shading represents the range of NLLEs in nine years for EA. (For interpretation of the references to colour in this figure legend, the reader is referred to the web version of this article.)

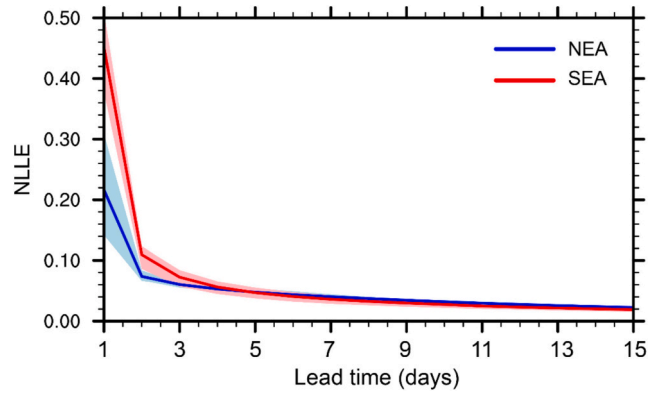

Fig. 3. Variations in the average NLLEs over northern and southern East Asia as a function of forecast lead-time. Blue and red shading represent the ranges of NLLEs in nine years for the NEA and SEA, respectively. (For interpretation of the references to colour in this figure legend, the reader is referred to the web version of this article.)

mainly west of 115°E. Negative NLLEs represent the decay of forecast errors relative to the initial errors. As the forecast time increases, the positive NLLEs tend to decrease to zero, and the negative NLLEs tend to increase to zero. That is, NLLEs over all NEA tend to approach zero. It should be noted that the NLLE value is always higher than zero, reflecting the statistical property of the dynamical system. However, in this study the number of ensemble members is 51, which may be not sufficient to reveal the statistical property of error growth dynamics for summer SAT over EA. Thus, the phenomenon of negative NLLEs occur. On the third day, NLLEs for most regions exhibit a sharp drop to lower than 0.08. Only a few regions, all located in the southeast part of NEA, have NLLEs that are higher than 0.08. The negative NLLEs become positive after the first 2 days, and the highest NLLEs are mainly in the northern, southern, and eastern regions of NEA. Smaller NLLEs occur mainly to the west of 115°E, where the NLLEs are initially negative. This spatial distribution of NLLEs lasts from the first day to the eighth day. On the ninth day, larger NLLEs are distributed mainly in the northeastern and eastern regions of NEA. The NLLEs continue to decrease as the lead-times increase. NLLEs are lower than 0.04 for all NEA by the ninth day; on fifth day, the NLLEs for NEA are lower than 0.03 and are lower than 0.02 for the northwestern regions of NEA. The evolutions of the NLLEs over 15 days show that the error growth rates have a heterogeneous distribution structure over NEA, with lower rates for some western and northwestern regions of NEA. Smaller NLLEs represent slow forecast error growth, so this indicates that regions with relatively smaller NLLEs contribute less to forecast errors. Regions with higher NLLEs are more sensitive to error growth and make a larger contribution to forecast errors, thereby constraining the upper limit for predictability. The forecast skill for these high-NLLE regions is also lower because of the higher error growth rates. Adding more observations for these regions and using more advanced data assimilation techniques may improve forecast skill.

Fig. 5 shows how the spatial distribution of NLLEs in SEA varies with time. As for NEA, NLLEs for SEA are largest on the first day and decrease with increasing forecast lead-time. However, in contrast to NEA, positive NLLEs are distributed over most of SEA on the first day, and very few regions have negative NLLEs. In general, NLLEs for SEA remain large during the first 2 days. On the third day, there is a large decrease in NLLEs for northern and southern regions of SEA, whereas NLLEs for central regions remain high. However, on the fourth day, NLLEs for the central region also decrease markedly. Also on the fourth day, NLLEs for some southern regions decrease to values <0.04, whereas those for most northern regions exceed 0.06. As the forecast lead-time increases, NLLEs continue to decrease for all of SEA. Between the sixth and ninth days, NLLEs remain higher than 0.04 for most northern regions and are smaller for southern regions. From the eleventh to the fifteenth day, NLLEs are smaller for all SEA compared with previous days, but NLLEs remain higher for northern regions than for southern regions. This shows that error growth rates also have a heterogeneous spatial distribution over SEA. In contrast to NEA, the lower error growth rates in SEA occur mainly in southern regions, whereas larger error growth rates occur mainly in northern regions. This shows that the northern regions of SEA are favorable for high forecast error growth, thereby constraining the upper limit for predictability. The evolution of the spatial structures of NLLEs over NEA and SEA with forecast lead-time shows that the distribution of error growth rates differs over the two areas. For NEA, high error growth rates occur mainly for the western and northwestern regions, whereas high error growth rates occur mainly for the northern regions of SEA. NEA and SEA therefore have different regions that are favorable for high forecast error growth.

Fig. 6 shows variations in SAT forecast error growth with lead-time, averaged over NEA and SEA. Although forecast error growths increase consistently with lead-time for both NEA and SEA, the growth patterns are different for the two regions throughout the forecast time. Initially, the average forecast error growth for NEA is slightly higher than 0.2, whereas the average forecast error growth for SEA is 0.45. Up to a lead-time of 5 days, the forecast error growth for NEA is always smaller than that for SEA. However, from the fifth day to the last day, the forecast error growth for NEA remains higher than that for SEA. This shows that the error growth dynamics differ between the two areas. The changes in forecast error growths for NEA and SEA correspond to error growth

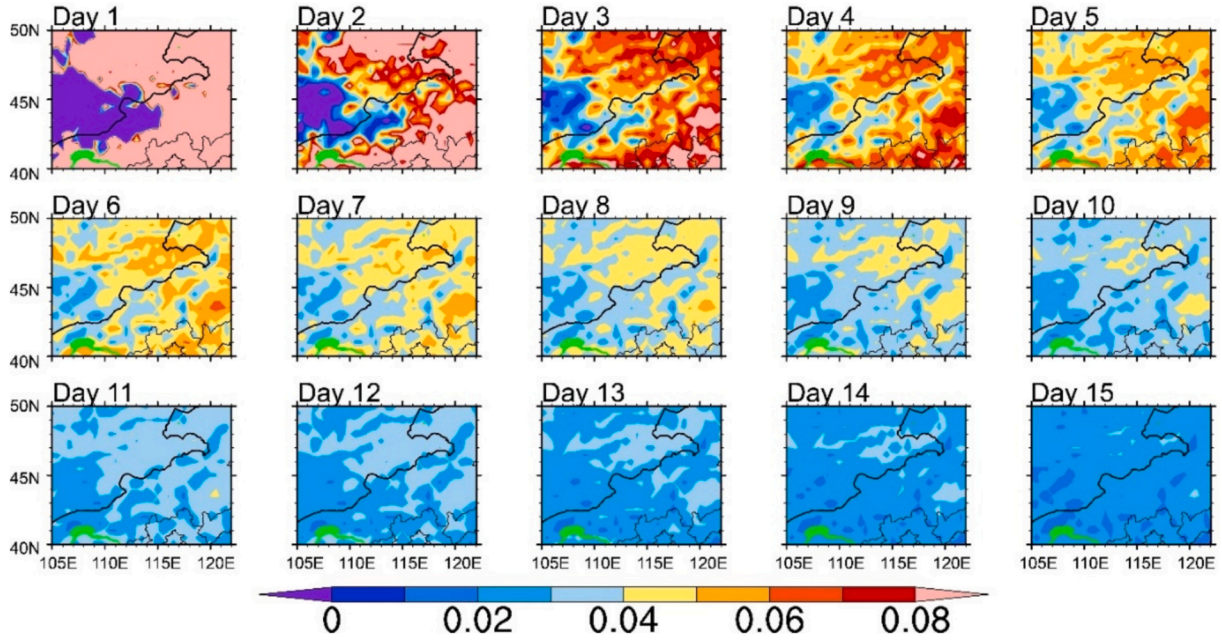

Fig. 4. Spatial distributions of NLLEs over NEA for each day in the 15-day forecast period. The green lines of each panel denote the Yellow River. (For interpretation of the references to colour in this figure legend, the reader is referred to the web version of this article.)

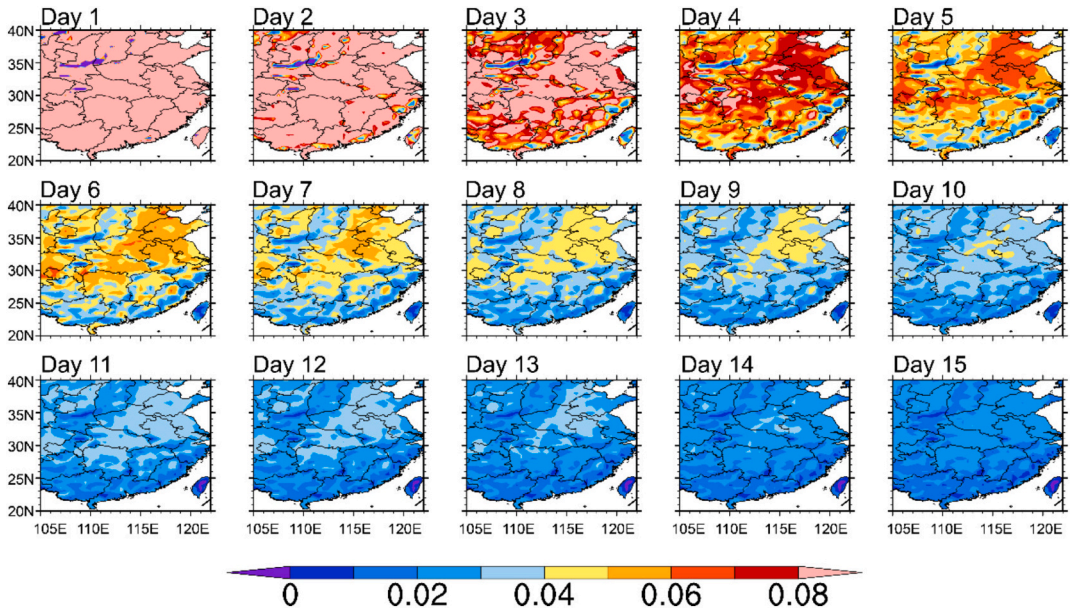

Fig. 5. Same as Fig. 4, but for SEA.

rates. The forecast error growth is obtained from the NLLE, multiplied by forecast lead-time. Hence, the error growth rates determine the forecast error growth. Initially, the average NLLEs for NEA and SEA are 0.21 and 0.45, respectively, which are the exact values for the forecast error growths for NEA and SEA, respectively. Up to a lead-time of 5 days, the error growth rate for NEA is always lower than that for SEA, and the forecast error growths for the two areas reflect this relationship. That is, the forecast error growth for NEA is always lower than that for SEA until the lead-time reaches 5 days. After the fifth day, the error growth rate for NEA exceeds that for SEA. Consequently, the forecast error growth for NEA also exceeds that for SEA. Although the two areas have different error growth dynamics, the forecast error growth reaches the saturation level on the thirteenth day for both areas. This indicates that the upper limit for predictability of summer SAT is 12 days, for both NEA and SEA, which is the same as that for all EA, thus indicating that the upper predictability limit for EA is robust.

After studying the average forecast error growths for NEA and SEA, we further explore the regional forecast error growths. Fig. 7 shows variations in the spatial distributions of forecast error growth for NEA with increasing forecast lead-time. In general, forecast error growths are smallest for all NEA on the first day and tend to increase with lead-time thereafter. In practice, the spatial structure of the forecast error growths corresponds to that for the spatial distribution of error growth rates. During the first two days, forecast error growths are negative to the west of 115°E, and this is attributed to the negative error growth rates for these areas. As the forecast lead-time increases, forecast error growths over these areas gradually approach zero. On the fourth day, forecast error growths become positive for all NEA; however, forecast error

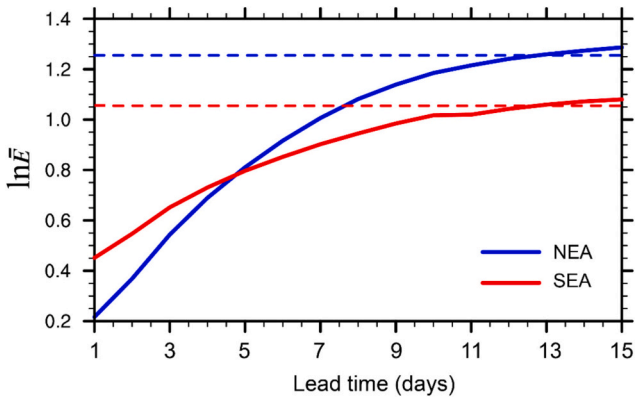

Fig. 6. Average forecast error growths (natural logarithm scale) over NEA and SEA as a function of forecast lead-time. Blue and red represent NEA and SEA, respectively. Dashed blue and red lines represent the saturation levels for NEA and SEA, respectively. (For interpretation of the references to colour in this figure legend, the reader is referred to the web version of this article.)

growths for areas that initially had negative values remain lower than those for the remaining areas. This structure persists from the first day to the tenth day. For the last 4 days of forecast lead-times, the spatial distribution of forecast error growth remains unchanged for all NEA. This is mainly because the forecast error growth has entered the random regime (Ding and Li, 2007). In the random regime, forecast error growths cease to increase and predictability is lost completely. In this random regime, high forecast error growths occur mainly in the northern, eastern, and southern regions of NEA, whereas the forecast error growths for some western and northwestern regions of NEA are low. The spatial structure of the forecast error growths corresponds to that for the error growth rates.

Fig. 8 shows variations in the spatial distribution of forecast error growths over SEA with increasing forecast lead-time. As for NEA, forecast error growths tend to increase with forecast lead-time for SEA. However, in contrast to NEA, forecast error growths are positive for most regions in SEA, and very few regions have negative forecast error growths. Forecast error growths increase with increasing forecast time and are largest for western regions of SEA on the third day. During the following days, the scope of larger forecast error growths extends and larger forecast error growths also occur for some central and northeastern regions of SEA. The forecast error growth for southern regions of SEA remains relatively small compared with other regions of SEA, although it also increases with lead-time. Forecast error growths generally reach high values and remain unchanged during the last 4 days. This is because the forecast error growths enter the random regime and predictability is lost completely. During the last 4 days, as for the previous 11 days, forecast error growths are greater for northern regions of SEA than for southern regions. This shows that northern regions of NEA are more favorable for forecast error growth than southern regions of NEA and is consistent with the spatial structure found for the evolution of error growth rates.

From Figs. 7 and 8, summer SAT over NEA and SEA exhibit distinct spatial structures of error growths. Previous studies have demonstrated that soil moisture exerts a substantial influence on temperature forecast skill. (e.g., Kanamitsu et al., 2003; Orth and Seneviratne, 2014). Soil moisture in East Asia is characterized by pronounced spatial heterogeneity. Previous research has pointed that soil moisture is markedly lower in NEA, whereas SEA exhibits substantially higher values (e.g. Cheng et al., 2015). In NEA, soil moisture deficit results in less water for latent heat flux. Hence, sensible heat flux increases and the atmosphere undergoes substantial heating. Consequently, the amplitude of daily SAT variability is significantly amplified, which is unfavorable for skillful performances of numerical models. This explains why forecast error growths of SAT over NEA, especially the northern regions of NEA, are quite large. In the SEA region, abundant soil moisture sustains a large latent-heat flux that effectively cools the atmosphere, resulting in suppressed daily SAT variability. Therefore, numerical models perform relatively better. That is, the error growths over SEA, especially the southern regions of SEA, are smaller. Therefore, from our perspective, soil moisture is key factor, which is responsible for differences in error growth structures over the two regions.

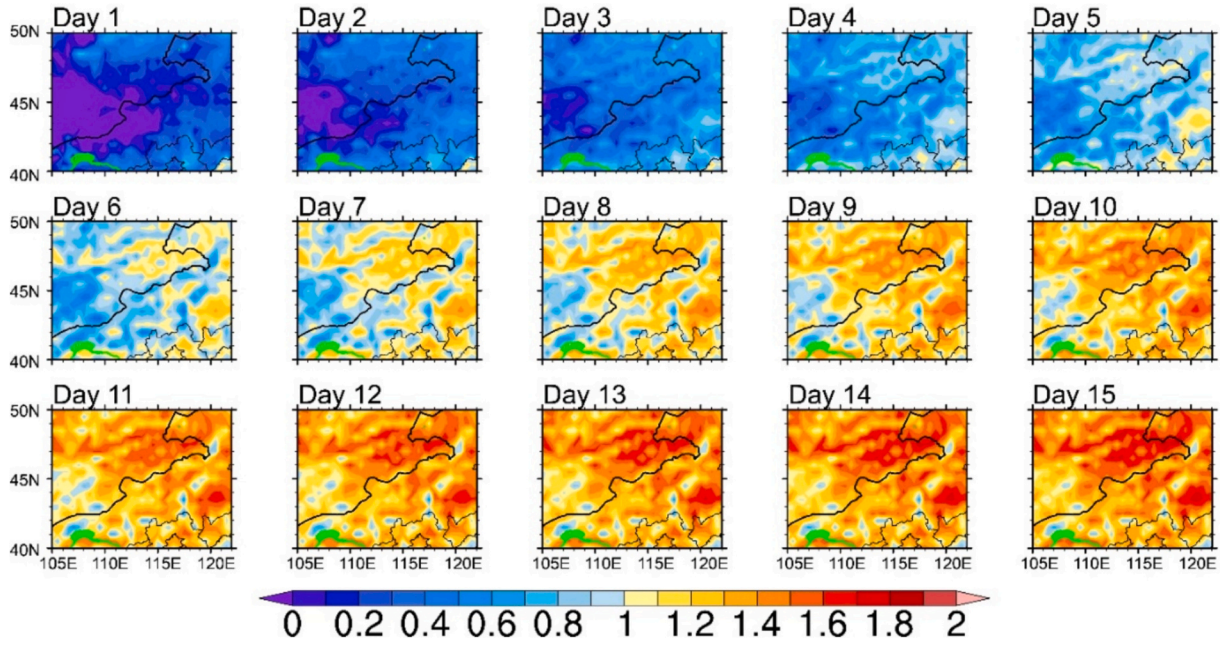

Fig. 7. Same as for Fig. 4, but for forecast error growth. The green lines of each panel denote the Yellow River. (For interpretation of the references to colour in this figure legend, the reader is referred to the web version of this article.)

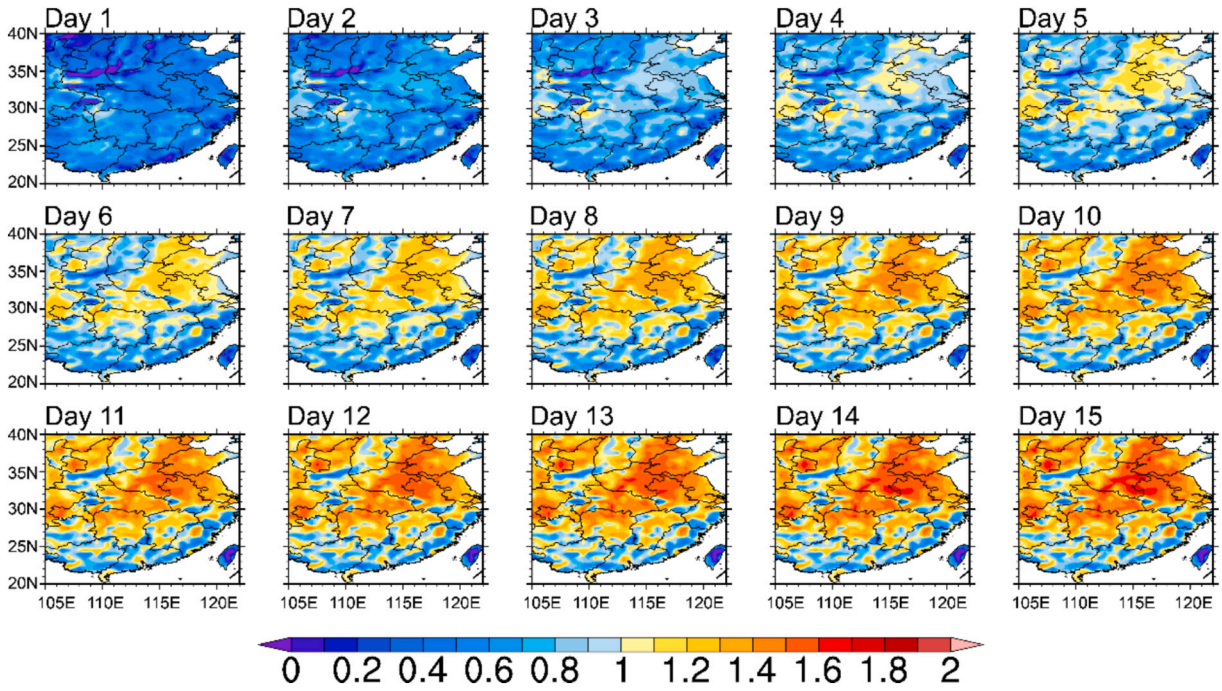

Fig. 8. Same as for Fig. 5, but for forecast error growth.

4. Conclusion and discussion

4.1. Conclusion

Publicly accessible accurate SAT forecasts are essential for society; however, multiple factors such as the chaotic nature of the atmosphere, external forcings, and model uncertainties have strong impacts on forecast skill. This makes it challenging to accurately forecast SAT and to determine the upper limit for SAT predictability. Many researchers have investigated SAT predictability at sub-seasonal, seasonal, and longer timescales. However, few studies have investigated SAT predictability at the synoptic timescale and quantitively estimated its upper limit. In this study, we have used the NLLE method to quantify SAT predictability at synoptic timescales over EA.

The NLLE is an effective method to study the predictability of dynamical systems (Li et al., 2020a, 2020b, 2021). Although the small amount of observation data posed challenges for identify reliable global analogues, limiting the direct application of NLLE method in atmospheric and oceanic sciences. The derivative of NLLE, local dynamic analogues method has overcome this difficulty by considering local condition in the search analogue of the complex, high-dimensional dynamical system. Using the local dynamic analogues method, the predictability of monthly precipitation, Madden–Julian Oscillation (MJO), Pacific decadal oscillation (PDO), the Atlantic multidecadal oscillation (AMO) has been quantitatively estimated (Ding et al., 2010, 2016; Liu et al., 2016; Hou et al., 2018, 2020, 2022; Mengist and Seo, 2022). Nowadays, the ensemble forecast technique is much prevailing in the operation and scientific research. In this study, we combined the NLLE method with ECMWF ensemble forecasts to investigate predictability and error growth dynamics for SAT over EA.

There was very little spread between the error growth rates over EA for each year. However, evolution of error growth rates in each year show similar varying tendency. The evolution tendency main can be classified into three different stages: a sharp decrease, a stable decrease, and a minor change. NLLEs at the sharp decrease and stable decrease stages are relatively larger, and change quite obviously. However, at the third stage, NLLEs seem to remain unchanged, although they still keep decreasing and approach towards zero. This interesting phenomenon of variations of NLLEs in three stages is not found in theoretical dynamical system (e.g. Lorenz models, logistic map and Hénon map), demonstrating the complexity of the modeled atmospheric system. We hold the opinion that the interesting phenomenon of variations of NLLEs is attributed to the inherent property of atmosphere. Previous studies pointed out that small forecast errors of atmosphere tend to double in about two days. As the forecast errors become larger the growth rate subsides (Dalcher and Kalnay, 1987; Lorenz, 1996; Kalnay, 2003). In this study, though the NLLE decreases continuously, it maintains a relatively high value for two forecast time days. After the second day, the growth rate changed slightly. Therefore, our findings support the views of previous research. Then, we quantify the upper predictability limit of SAT over EA based on the alternative method. The rational of estimating predictability is to study the evolution of the error growth. That is, the error growth undergoes linear and nonlinear regimes before reaching the saturation level, and the event is predictable. Once the saturation level is reached, the error growth evolved in the random phase and the predictability is lost completely. Therefore, based on this rational, the upper predictability limit for summer SAT over EA is determined to be 12 days. In addition, spatial structures of error growth and its rate are investigated to better understand error growth dynamics over EA. The error growth rates in both NEA and SEA have a spatially heterogeneous distribution. Some western and northwestern regions of NEA have smaller error growth rates than other regions, whereas southern regions of SEA have smaller error growth rates than northern regions. The spatial structures of forecast error growths show that small forecast error growths are distributed mainly in some western and northwestern regions of NEA and in southern regions of SEA. High error growth rates indicate a constraint on the predictability limit and a limitation for forecast skill. More projects of target observations for regions with high error growth rates may result in higher predictability and forecast skill.

4.2. Discussion

Nowadays, the ensemble forecast technique is much prevailing in the operation and scientific research. Taking into account the advantages of ensemble forecasting, we introduced an approach to directly calculate

the NLLE from ensemble forecasts and observation data without having to find local dynamic analogues for reference conditions. Therefore, this approach of using ensemble forecasts is an alternative method to quantify the predictability of atmospheric and oceanic variables. However, it should be noted that the predictability limits of SAT over EA are obtained from the multi-ensemble modeling system of ECMWF. It manifests that the outcome is inevitably affected by the model uncertainties. Incomplete understanding of atmospheric dynamics, parameterizations of sub-grid scale microphysical processes and low model resolution are mainly responsible for the presence of the model uncertainties. There is no doubt that these factors will underestimate the predictability limits of SAT over EA. Hence, the effects of model uncertainties are the limitations of the alternative method based on ensemble forecasts. In addition, the initial condition errors are determined by the observational errors and the adopted data assimilation technique. Using different techniques assimilating the observational errors, the initial condition errors may vary, further affecting the calculation of NLLE and predictability limits. Other sources, such as selection of forecast lead times and number of ensemble members, exert some degree of influence on predictability limits. In future work, how to reduce these sources of uncertainties such as improving the resolution and performing the targeted observations is a challenging but worthwhile task.

Besides, we obtain that the upper predictability limit for summer SAT over EA is 12 days. This result demonstrates the forecasting capability of current numerical dynamical models. In addition, this study also overcomes the limitations of qualitative or linear research approaches by previous studies (Lee et al., 2013; Ehsan et al., 2019). Lorenz (1969) pointed out that the predictability limit of atmosphere at synoptic scale is roughly two weeks, indicating that current numerical dynamical models still have significant potential for enhancement. For example, providing more accurate initial conditions will be conducive to obtain higher upper limit of SAT predictability. Furthermore, this study shows distinct spatial structures of error growths over EA. We speculate that the soil moisture is a key factor the spatial heterogeneity of error growths. It means that soil moisture governs the dynamics of SAT evolution over EA. Therefore, improving soil moisture parameterization scheme is likely to yield more skillful forecasts.

Overall, this work introduces an alternative method for quantifying predictability, serving to broaden the scope of analytical techniques available. And it is promising to play a more essential role in the fields of atmospheric and oceanic predictability.

CRediT authorship contribution statement

Xuan Li: Writing – review & editing, Writing – original draft, Funding acquisition, Formal analysis, Conceptualization. **Xinyue Zhang:** Writing – review & editing, Visualization, Validation, Data curation. **Ruiqiang Ding:** Writing – review & editing, Visualization, Validation, Methodology. **Jianping Li:** Writing – review & editing, Visualization, Validation, Methodology. **Xiaowei Huai:** Writing – review & editing, Funding acquisition.

Declaration of competing interest

The authors declare that they have no known competing financial interests or personal relationships that could have appeared to influence the work reported in this paper.

Acknowledgments

This work is based on ensemble forecast data from the TIGGE project. The TIGGE is an initiative of the World Weather Research Programme (WWRP). This work was jointly supported by the National Natural Science Foundation of China (Grant Nos. 42575063, 62341133 and 42505061) and the Fundamental Research Funds for the Central Universities (Grant No. D5000240074). The authors have no relevant financial or non-financial interests to disclose.

Data availability

The TIGGE (The Interactive Grand Global Ensemble) (https://apps.ecmwf.int/datasets/data/tigge/levtype=sfc/type=pf/). The ERA-interim analysis is from (https://apps.ecmwf.int/datasets/data/interim-full-daily/levtype=sfc/), respectively.

References

Bougeault, P., Coauthors, 2010. The THORPEX interactive grand global ensemble. Bull. Am. Meteorol. Soc. 91, 1059–1072.
Budikova, D., 2009. Role of Arctic sea ice in global atmospheric circulation: a review. Glob. Planet. Chang. 68, 149–163.
Cheng, S., Guan, X., Huang, J., et al., 2015. Long-term trend and variability of soil moisture over East Asia. J. Geophys. Res. Atmos. 120 (17), 8658–8670.
Chou, J.F., 1989. Predictability of the atmosphere. Adv. Atmos. Sci. 6, 335–346.
Dalcher, A., Kalnay, E., 1987. Error growth and predictability in operational ECMWF forecasts. Tellus A 39, 474–491.
Dee, D.P., Coauthors, 2011. The ERA-interim reanalysis: configuration and performance of the data assimilation system. Q. J. R. Meteorol. Soc. 137, 553–597.
Dickinson, R.E., 1995. Land-atmosphere interaction. Rev. Geophys. 33, 917–922.
Ding, R.Q., Li, J.P., 2007. Nonlinear finite-time Lyapunov exponent and predictability. Phys. Lett. A 364, 396–400.
Ding, R.Q., Li, J.P., Seo, K.H., 2010. Predictability of the Madden–Julian Oscillation estimated using observational data. Mon. Weather Rev. 138, 1004–1013.
Ding, R.Q., Li, J.P., Seo, K.H., 2011. Estimate of the predictability of boreal summer and winter intraseasonal oscillations from observations. Mon. Weather Rev. 139, 2421–2438.
Ding, R.Q., Li, J.P., Zheng, F., Feng, J., Liu, D.Q., 2016. Estimating the limit of decadal-scale climate predictability using observational data. Clim. Dyn. 46, 1563–1580.
Ehsan, M.A., Kucharski, F., Almazroui, M., Ismail, M., Tippett, M.K., 2019. Potential predictability of Arabian Peninsula summer surface air temperature in the North American multimodel ensemble. Clim. Dyn. 53, 4249–4266.
Fan, H., Wang, L., Zhang, Y., et al., 2020. Predictable patterns of wintertime surface air temperature in Northern Hemisphere and their predictability sources in the SEAS5. J. Clim. 33 (24), 10743–10754.
Farrell, B.F., 1990. Small error dynamics and the predictability of atmospheric flows. J. Atmos. Sci. 47, 2409–2416.
Froude, L.S.R., 2010. TIGGE: comparison of the prediction of Northern Hemisphere extratropical cyclones by different ensemble prediction systems. Weather Forecast. 25 (3), 819–836.
He, W., Xie, X., Mei, Y., Wan, S., Zhao, S., 2021. Decreasing predictability as a precursor indicator for abrupt climate change. Clim. Dyn. 56, 3899–3908.
Hersbach, H., Bell, B., Berrisford, P., et al., 2020. The ERA5 global reanalysis. Q. J. R. Meteorol. Soc. 146 (730), 1999–2049.
Hou, Z., Li, J., Ding, R., et al., 2018. Asymmetry of the predictability limit of the warm ENSO phase. Geophys. Res. Lett. 45 (15), 7646–7653.
Hou, Z., Zuo, B., Zhang, S., et al., 2020. Model forecast error correction based on the local dynamical analog method: an example application to the ENSO forecast by an intermediate coupled model. Geophys. Res. Lett. 47 (19), e2020GL088986.
Hou, Z., Li, J., Ding, R., et al., 2022. Investigating decadal variations of the seasonal predictability limit of sea surface temperature in the tropical Pacific. Clim. Dyn. 59 (3), 1079–1096.
Jia, L., DelSole, T., 2012. Multi-year predictability of temperature and precipitation in multiple climate models. Geophys. Res. Lett. 39 (17).
Jin, F.-F., 1996. Tropical ocean-atmosphere interaction, the Pacific cold tongue, and the El Niño-Southern Oscillation. Science 274, 76–78.
Kalnay, E., 2003. Atmospheric Modeling, Data Assimilation and Predictability. Cambridge University Press.
Kanamitsu, M., Lu, C.H., Schemm, J., et al., 2003. The predictability of soil moisture and near-surface temperature in hindcasts of the NCEP seasonal forecast model. J. Clim. 16 (3), 510–521.
Kirtman, B.P., Coauthors, 2014. The North American multimodel ensemble: phase-1 seasonal-to-interannual prediction; phase-2 toward developing intraseasonal prediction. Bull. Am. Meteorol. Soc. 95, 585–601.
Lee, J.Y., Lee, S.S., Wang, B., et al., 2013. Seasonal prediction and predictability of the Asian winter temperature variability. Clim. Dyn. 41 (3), 573–587.
Li, J.P., Ding, R.Q., 2011. Temporal–spatial distribution of atmospheric predictability limit by local dynamical analogs. Mon. Weather Rev. 139, 3265–3283.
Li, J.P., Ding, R.Q., 2013. Temporal-spatial distribution of the predictability limit of monthly sea surface temperature in the global oceans. Int. J. Climatol. 33, 1936–1947.
Li, X., Ding, R., Li, J., 2020a. Quantitative study of the relative effects of initial condition and model uncertainties on local predictability in a nonlinear dynamical system. Chaos, Solitons Fractals 139, 110094.
Li, X., Ding, R., Li, J., 2020b. Quantitative comparison of predictabilities of warm and cold events using the backward nonlinear local Lyapunov exponent method. Adv. Atmos. Sci. 37 (9), 951–958.

Li, X., Feng, J., Ding, R., et al., 2021. Application of backward nonlinear local lyapunov exponent method to assessing the relative impacts of initial condition and model errors on local backward predictability. Adv. Atmos. Sci. 38 (9), 1486–1496.
Liang, P., Lin, H., 2018. Sub-seasonal prediction over East Asia during boreal summer using the ECCC monthly forecasting system. Clim. Dyn. 50, 1007–1022.
Liu, J., Li, W., Chen, L., et al., 2016. Estimation of the monthly precipitation predictability limit in China using the nonlinear local Lyapunov exponent. J. Meteorol. Res. 30 (1), 93–102.
Liu, Z., Zhou, W., Zhang, R., et al., 2022. Global-scale interpretable drought reconstruction utilizing anomalies of atmospheric dynamics. J. Hydrometeorol. 23 (9), 1507–1524.
Liu, Z., Zhou, W., Wang, X., 2024. Extreme meteorological drought events over China (1951–2022): migration patterns, diversity of temperature extremes, and decadal variations. Adv. Atmos. Sci. 41 (12), 2313–2336.
Lorenz, E.N., 1963. Deterministic nonperiodic flow. J. Atmos. Sci. 20, 130–141.
Lorenz, E.N., 1965. A study of the predictability of a 28-variable atmospheric model. Tellus 17, 321–333.
Lorenz, E.N., 1969. Atmospheric predictability as revealed by naturally occurring analogues. J. Atmos. Sci. 26, 636–646.
Lorenz, E.N., 1996. Predictability: a problem partly solved. Proc. Semin. Predictabil. 1 (1), 1–18.
Mengist, C.K., Seo, K.H., 2022. How long can the MJO be predicted during the combined phases of ENSO and QBO? Geophys. Res. Lett. 49 (8), e2022GL097752.
Monerie, P.-A., Robson, J., Dong, B., Dunstone, N., 2018. A role of the Atlantic Ocean in predicting summer surface air temperature over North East Asia? Clim. Dyn. 51, 473–491.
Müller, W.A., Baehr, J., Haak, H., et al., 2012. Forecast skill of multi-year seasonal means in the decadal prediction system of the Max Planck Institute for meteorology. Geophys. Res. Lett. 39 (22).
Nese, J.M., 1989. Quantifying local predictability in phase space. Phys. D 35, 237–250.
Orth, R., Seneviratne, S.I., 2014. Using soil moisture forecasts for sub-seasonal summer temperature predictions in Europe. Clim. Dyn. 43 (12), 3403–3418.
Rohini, P., Rajeevan, M., 2023. An analysis of prediction skill of heat waves over India using TIGGE ensemble forecasts. Earth Space Sci. 10 (3), e2020EA001545.
Salvi, K., Villarini, G., Vecchi, G.A., et al., 2017. Decadal temperature predictions over the continental United States: analysis and enhancement. Clim. Dyn. 49 (9), 3587–3604.
Stefanova, L., Misra, V., O'Brien, J.J., Chassignet, E.P., Hameed, S., 2012. Hindcast skill and predictability for precipitation and two-meter air temperature anomalies in global circulation models over the Southeast United States. Clim. Dyn. 38, 161–173.
Su, X., Yuan, H., Zhu, Y., et al., 2014. Evaluation of TIGGE ensemble predictions of Northern Hemisphere summer precipitation during 2008–2012. J. Geophys. Res. Atmos. 119 (12), 7292–7310.
Swinbank, R., Coauthors, 2016. The TIGGE project and its achievements. Bull. Am. Meteorol. Soc. 97, 49–67.
Thompson, P.D., 1957. Uncertainty of initial state as a factor in the predictability of large scale atmospheric flow patterns. Tellus 9, 275–295.
Vannitsem, S., 2017. Predictability of large-scale atmospheric motions: Lyapunov exponents and error dynamics. Chaos 27, 032101.
Verfaillie, D., Doblas-Reyes, F.J., Donat, M.G., et al., 2021. How reliable are decadal climate predictions of near-surface air temperature? J. Clim. 34 (2), 697–713.
Vitart, F., Coauthors, 2017. The subseasonal to seasonal (S2S) prediction project database. Bull. Am. Meteorol. Soc. 98, 163–173.
Wolf, A., Swift, J.B., Swinney, H.L., Vastano, J.A., 1985. Determining Lyapunov exponents from a time series. Phys. D 16, 285–317.
Xiang, B., Sun, Y.Q., Chen, J.H., Johnson, N.C., Jiang, X., 2020. Subseasonal prediction of land cold extremes in boreal wintertime. J. Geophys. Res.-Atmos. 125, e2020JD032670.
Yoden, S., Nomura, M., 1993. Finite-time Lyapunov stability analysis and its application to atmospheric predictability. J. Atmos. Sci. 50, 1531–1543.